TMEM16A and TMEM16B channel proteins generate Ca^{2+}-activated Cl^- current and regulate melatonin secretion in rat pineal glands

Received for publication, October 7, 2017, and in revised form, November 28, 2017 Published, Papers in Press, November 29, 2017, DOI 10.1074/jbc.RA117.000326

Hisao Yamamura[1], **Kaori Nishimura, Yumiko Hagihara, Yoshiaki Suzuki, and Yuji Imaizumi**

From the Department of Molecular and Cellular Pharmacology, Graduate School of Pharmaceutical Sciences, Nagoya City University, Nagoya 467-8603, Japan

Edited by Roger J. Colbran

Pinealocytes regulate circadian rhythm by synthesizing and secreting melatonin. These cells generate action potentials; however, the contribution of specific ion channels to melatonin secretion from pinealocytes remains unclear. In this study, the involvement and molecular identity of Ca^{2+}-activated Cl^- (Cl_{Ca}) channels in the regulation of melatonin secretion were examined in rat pineal glands. Treatment with the Cl_{Ca} channel blockers, niflumic acid or $T16A_{inh}$-A01, significantly reduced melatonin secretion in pineal glands. After pineal K^+ currents were totally blocked under whole-cell patch clamp conditions, depolarization and subsequent repolarization induced a slowly activating outward current and a substantial inward tail current, respectively. Both of these current changes were dependent on intracellular Ca^{2+} concentration and inhibited by niflumic acid and $T16A_{inh}$-A01. Quantitative real-time PCR, Western blotting, and immunocytochemical analyses revealed that TMEM16A and TMEM16B were highly expressed in pineal glands. siRNA knockdown of TMEM16A and/or TMEM16B showed that both channels contribute to Cl_{Ca} currents in pinealocytes. Conversely, co-expression of TMEM16A and TMEM16B channels or the expression of this tandem channel in HEK293 cells mimicked the electrophysiological characteristics of Cl_{Ca} currents in pinealocytes. Moreover, bimolecular fluorescence complementation, FRET, and co-immunoprecipitation experiments suggested that TMEM16A and TMEM16B can form heteromeric channels, as well as homomeric channels. In conclusion, pineal Cl_{Ca} channels are composed of TMEM16A and TMEM16B subunits, and these fluxes regulate melatonin secretion in pineal glands.

Pineal glands regulate the circadian rhythm through the synthesis and secretion of melatonin. This melatonin production can be either positively or negatively regulated by sympathetic and parasympathetic systems, respectively. Norepinephrine (NE)[2] stimulates adrenergic β_1 receptor and promotes cAMP production. The cAMP activates a melatonin-synthesizing enzyme, arylalkylamine-*N*-acetyltransferase, thus promoting melatonin biosynthesis from tryptophan in pinealocytes. NE also stimulates adrenergic α_1 receptor leading to inositol 1,4,5-trisphosphate-induced Ca^{2+} release, which is thought to enhance the adrenergic β_1 signal pathway (1). In addition to this adrenergic regulation, there is parasympathetic innervation in pineal glands (2). Acetylcholine (ACh) activates nicotinic ACh receptors. This elicits membrane depolarization, and then induces Ca^{2+} influx through voltage-dependent Ca^{2+} channels (VDCCs). The resulting increase in intracellular Ca^{2+} concentration ($[Ca^{2+}]_i$) causes an exocytosis of glutamate (3). This glutamate stimulates metabotropic glutamate receptor type 3 and thus decreases cAMP production, resulting in the reduction of arylalkylamine-*N*-acetyltransferase activity and melatonin synthesis (4).

Mammalian pinealocytes can generate action potentials (5–9) and, pineal glands express several types of ion channels, including voltage-dependent K^+ channels (7, 10), Ca^{2+}-activated K^+ channels (11–13), non-selective cation channels (14), and store-operated Ca^{2+} channels (12), in addition to VDCCs (7, 9, 11). However, there has been no detailed analysis of the possibility that there is functional expression of anion channels.

Ca^{2+}-activated Cl^- (Cl_{Ca}) channels play important roles in many physiological processes, such as epithelial secretion, sensory transduction, neuronal signaling, cardiac excitability, and smooth muscle contraction. Two TMEM16 family proteins, TMEM16A and TMEM16B, have been identified as functional Cl_{Ca} channels (15–17). TMEM16A is widely expressed in a large variety of tissues, including secretory epithelial cells, smooth muscle cells, interstitial cells of Cajal, and nociceptive neurons. On the other hand, the findings of TMEM16B expression have been limited in sensory nervous systems, such as olfactory neurons and retinal photoreceptors (18–20).

The present study was undertaken to study the expression of the Cl_{Ca} channel, elucidate their molecular entity, and demonstrate their involvement in melatonin secretion in rat pineal

This work was supported by Grant-in-Aid for Scientific Research on Innovative Areas 17H05537 (to H. Y.), Grant-in-Aid for Scientific Research (B) 26293021 (to Y. I.), and Grants-in-Aid for Scientific Research (C) 25460104 and 16K08278 (to H. Y.) from the Japan Society for the Promotion of Science. The authors declare that they have no conflicts of interest with the contents of this article.

[1] To whom correspondence should be addressed: 3-1 Tanabedori Mizuhoku, Nagoya 467-8603, Japan. Tel.: 81-52-836-3433; Fax: 81-52-836-3470; E-mail: yamamura@phar.nagoya-cu.ac.jp.

[2] The abbreviations used are: NE, norepinephrine; ACh, acetylcholine; BiFC, bimolecular fluorescent complementation; $[Ca^{2+}]_{pip}$, Ca^{2+} concentration in the pipette solution; Cl_{Ca} channel, Ca^{2+}-activated Cl^- channel; E_{FRET}, efficiency of FRET; τ_{act}, time constant for current activation; τ_{tail}, time constant for tail current deactivation; TIRF, total internal reflection fluorescence; VDCC, voltage-dependent Ca^{2+} channel; Ω, ohm.

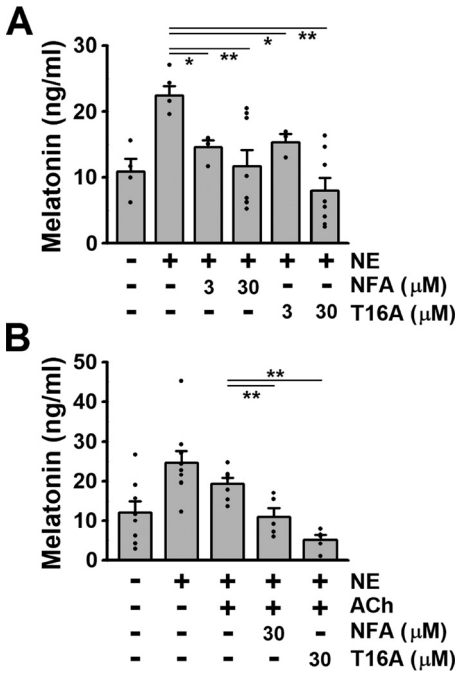

Figure 1. Involvement of Cl_{Ca} channel activity on melatonin secretion. *A,* effects of Cl_{Ca} channel blockers on melatonin secretion via sympathetic stimulation. Melatonin secretion induced by 1 μM NE was reduced by 3 and 30 μM niflumic acid (*NFA*) or $T16A_{inh}$-A01 (T16A). *B,* effects of Cl_{Ca} channel blockers on NE-induced melatonin secretion in the presence of parasympathetic stimulation. In the presence of both 1 μM NE and 100 μM ACh, blockade of Cl_{Ca} channels by 30 μM niflumic acid or $T16A_{inh}$-A01 attenuated melatonin secretion. Experimental data were obtained from 3 to 9 pineal glands. *, $p < 0.05$; **, $p < 0.01$ by Tukey's test.

glands. To our knowledge, our results are the first to report that TMEM16A and TMEM16B proteins are functionally expressed as Cl_{Ca} channels, and that this Cl^- current contributes to the regulation of melatonin secretion in mammalian pineal glands.

Results

Possible involvement of Cl_{Ca} channel activity in melatonin secretion

At first, effects of Cl_{Ca} channel blockers on melatonin secretion under the regulation by sympathetic and/or parasympathetic pathways were examined in rat pineal glands using a melatonin ELISA assay kit. Application of 1 μM NE caused a significant increase in melatonin secretion (22.5 ± 1.5 ng/ml, $n = 5$, $p = 0.019$ ($F = 5.71$) *versus* control of 10.9 ± 2.0 ng/ml, $n = 4$, by Tukey's test) (Fig. 1*A*). Pretreatment with niflumic acid, a classical Cl_{Ca} channel blocker, reduced the NE-induced melatonin secretion in a concentration-dependent manner (3 μM, 14.6 ± 1.0 ng/ml, $n = 4$, $p = 0.041$ *versus* NE; 30 μM, 11.8 ± 2.4 ng/ml, $n = 8$, $p = 0.009$). Application of $T16A_{inh}$-A01, a specific blocker of TMEM16A and TMEM16B Cl_{Ca} channels, also dose-dependently reduced the NE-induced melatonin secretion (3 μM, 15.4 ± 1.2 ng/ml, $n = 3$, $p = 0.016$; 30 μM, 8.0 ± 1.9 ng/ml, $n = 8$, $p = 0.0003$). These Cl_{Ca} channel blockers did not affect melatonin secretion in the absence of NE (data not shown). On the other hand, the NE-induced melatonin secretion was attenuated by addition of 100 μM ACh, which mimics parasympathetic stimulation (19.3 ± 1.5 ng/ml, $n = 7$) (Fig. 1*B*). In the presence of ACh, application of 30 μM niflumic acid (11.0 ± 2.2 ng/ml, $n = 5$, $p = 0.008$ ($F = 8.56$) *versus* NE + ACh by Tukey's test) or $T16A_{inh}$-A01 (5.2 ± 1.2 ng/ml, $n = 5$, $p = 0.00004$) further reduced the NE-induced melatonin secretion. These results indicate that the activity of Cl_{Ca} channels is involved in the regulation of melatonin secretion via sympathetic and parasympathetic pathways in rat pineal glands.

Cl^- currents and their sensitivity to Ca^{2+} in pinealocytes

Cl^- currents were measured in pinealocytes isolated from rat pineal glands, by use of K^+-deficient and Cl^--rich solutions under whole-cell voltage-clamp conditions (see "Experimental procedures"). Single pinealocytes were depolarized from the holding potential of −40 mV to selected test potentials (−80 ~ +100 mV) by +20 mV increment for 500 ms and, then repolarized to −80 mV for 250 ms every 15 s. The cell capacitance was 20.6 ± 0.8 pF ($n = 65$). When Ca^{2+} concentration in the pipette solution ($[Ca^{2+}]_{pip}$) was fixed to *p*Ca 6.0, time-dependent outward currents over ~400 pA in peak amplitude were detected at membrane potentials positive to +40 mV (I_{peak} = 59.3 ± 9.3 pA/pF at +100 mV, $n = 8$) (Fig. 2, *A* and *B*). Upon repolarization, characteristic inward tail currents were recorded (I_{tail} = 53.1 ± 7.4 pA/pF, $n = 8$). The current-voltage relationship shows that the reversal potential was ~0 mV (Fig. 2*B*). The amplitude of outward and tail currents were substantially reduced by the decrease in $[Ca^{2+}]_{pip}$ to *p*Ca 6.5 or 7.0, in a $[Ca^{2+}]_{pip}$-dependent manner ($n = 5$~10) (Fig. 2, *A–C*). The time constant for current activation (τ_{act}) at +100 mV and that for tail current deactivation (τ_{tail}) at −80 mV after +100 mV stimulation were 80.5 ± 8.4 and 81.0 ± 8.9 ms, respectively (n = 8) (Fig. 2, *D* and *E*). The τ_{act} and τ_{tail} were also affected by the $[Ca^{2+}]_{pip}$ change ($n = 5$~10) (Fig. 2, *D* and *E*). These data indicate that Cl^- channel activity in pinealocytes strongly depends upon $[Ca^{2+}]_i$.

Sensitivity to Cl_{Ca} channel blockers on pineal Cl^- currents

Effects of Cl_{Ca} channel blockers, niflumic acid, and $T16A_{inh}$-A01, on both outward and tail currents were examined in rat pinealocytes. When $[Ca^{2+}]_{pip}$ was *p*Ca 6.0, 6.5, and 7.0, the application of 100 μM niflumic acid significantly reduced the outward peak currents (10.5 ± 3.2 pA/pF at +100 mV and *p*Ca 6.0, $n = 10$, $p = 0.00003$ (F = 7.73) *versus* control of 53.4 ± 6.0 pA/pF by Student's *t* test, paired) (Fig. 3, *A* and *B*). The tail currents were also significantly reduced by 100 μM niflumic acid (15.7 ± 3.5 pA/pF at −80 mV after +100 mV stimulation and *p*Ca 6.0, $n = 10$, $p = 0.00003$ (F = 7.71) *versus* control of 50.2 ± 6.8 pA/pF), except when $[Ca^{2+}]_{pip}$ was *p*Ca 7.0. The inhibitory effect of niflumic acid on outward currents at $[Ca^{2+}]_{pip}$ of *p*Ca 6.0, was dose-dependent with an IC_{50} of 2.6 μM and the Hill coefficient of 0.81 ($n = 7$) (Fig. 3, *C*, *D*, and *G*). In addition, the outward and tail currents were also significantly inhibited by 10 μM $T16A_{inh}$-A01 ($n = 3$, $p = 0.024$ ($F = 6.38$) and $p = 0.012$ ($F = 8.95$), respectively, by Student's *t* test, paired) and the inhibition was removed by washout (Fig. 3, *E–G*). These data indicate that Cl_{Ca} currents sensitive to niflumic acid and $T16A_{inh}$-A01 are functionally expressed in rat pinealocytes.

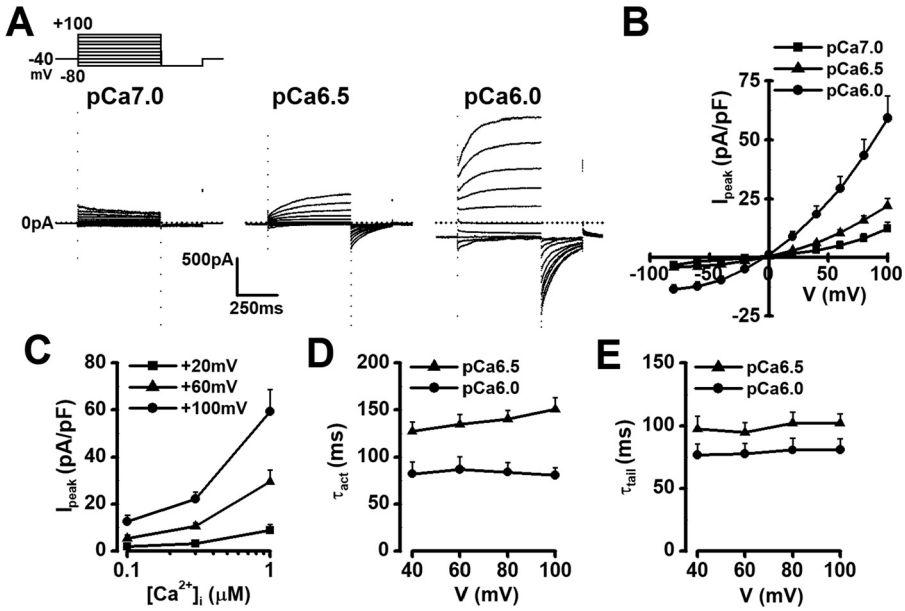

Figure 2. Macroscopic Cl_{Ca} currents in rat pinealocytes. *A*, in whole-cell voltage-clamp experiments, single pinealocytes were depolarized from the holding potential of −40 mV to test potentials (−80 ~ +100 mV) by +20 mV increment for 500 ms and subsequently repolarized to −80 mV for 250 ms every 15 s. Representative current traces of *p*Ca 7.0, 6.5, and 6.0 in the pipette solution. Note that time-dependent outward currents and tail currents, which are characteristic of Cl_{Ca} currents, were observed at *p*Ca 6.5 and 6.0 in pinealocytes. *B*, current-voltage relationships of outward currents at *p*Ca 7.0, 6.5, and 6.0. Note that these currents reversed around 0 mV, which is a theoretical equilibrium potential of Cl^- under the experimental conditions. *C*, Ca^{2+} dependence of outward currents. *D*, τ_{act} of outward currents. *E*, τ_{tail} of tail currents. Experimental data were obtained from 5 to 10 pinealocytes.

Possible contribution of Cl_{Ca} channel activity to the resting membrane potential

Effect of Cl_{Ca} channel blocker on the resting membrane potential was examined in rat pinealocytes under whole-cell current-clamp mode. The mean resting membrane potential was −34.5 ± 3.1 mV (n = 8) (Fig. 4). Application of 100 μM niflumic acid caused a significant hyperpolarization to −40.0 ± 2.8 mV (p = 0.007 (F = 3.77), n = 8, by Student's t test, paired) and it was recovered by removal of niflumic acid (to −30.5 ± 4.6 mV, n = 8, p = 0.043 (F = 2.47) *versus* niflumic acid, p = 0.163 (F = 1.56) *versus* control). The experimental conditions of the pipette solution used here provide Cl^- reversal potential of 0 mV and also the $[Ca^{2+}]_i$ lower than 100 nM. These may result in somewhat over and under estimation of the contribution, respectively. Thus, niflumic acid-sensitive Cl_{Ca} channel activity may be involved in the regulation of resting membrane potential in rat pinealocytes, particularly when $[Ca^{2+}]_i$ is elevated.

Expression of TMEM16A and TMEM16B in pineal glands

To identify the molecular components of Cl_{Ca} channels in rat pinealocytes, expression analyses of the TMEM16 family were performed by quantitative real-time PCR, Western blotting, and immunocytochemical methods. Among the TMEM16 family, *Tmem16B* mRNA was highly expressed (0.074 ± 0.009 of β-actin, n = 10), and *Tmem16A* and *Tmem16K* mRNAs were also identified in pineal glands (0.043 ± 0.007 and 0.061 ± 0.008, respectively, n = 10) (Fig. 5*A*). Western blot analysis showed the expression of TMEM16A and TMEM16B in the plasma membrane fraction from pineal glands (n = 6~8; Fig. 5*B*). In addition, immunocytochemical staining showed that TMEM16A and TMEM16B proteins were abundantly expressed at the plasma membrane of pinealocytes (n = 10) (Fig. 5*C*). Taken together, TMEM16A and TMEM16B are both expressed at the plasma membrane of rat pinealocytes.

siRNA knockdown of Tmem16A and Tmem16B in pinealocytes

We performed the siRNA knockdown of *Tmem16A* and *Tmem16B* in rat pinealocytes in an attempt to obtain direct evidence that the Cl_{Ca} currents were mediated by TMEM16A and/or TMEM16B channels. The selectivity of *Tmem16A* and *Tmem16B* siRNAs was confirmed by the quantitative real-time PCR method (Fig. 6*A*). In pinealocytes treated with control siRNA, the electrophysiological parameters of Cl_{Ca} currents (Fig. 6, *B–F*) were identical to those of native pinealocytes (Fig. 2). Cl_{Ca} currents in pinealocytes transfected with *Tmem16A* siRNA (65.1 ± 8.7% decrease at mRNA expression level, n = 4) showed significantly smaller amplitude (I_{peak} = 49.5 ± 2.5 pA/pF, n = 7, p = 0.042 (F = 16.29) *versus* control siRNA of 74.1 ± 8.7 pA/pF, n = 10, by Tukey's test; I_{tail} = 34.4 ± 2.6 pA/pF, p = 0.003 (F = 29.39) *versus* control siRNA of 50.3 ± 3.5 pA/pF, by Tukey's test) (Fig. 6, *B–D*), and also shorter τ_{act} and τ_{tail} values in comparison with those in control siRNA-treated pinealocytes (τ_{act} = 28.8 ± 2.6 ms at +100 mV, n = 7, p = 0.034 (F = 23.20) *versus* control siRNA of 95.9 ± 22.7 ms, n = 10, by Tukey's test; τ_{tail} = 15.5 ± 1.4 ms at −80 mV after +100 mV stimulation, p = 0.046 (F = 11.72) *versus* control siRNA of 79.6 ± 23.0 ms, by Tukey's test) (Fig. 6, *B*, *E*, and *F*). *Tmem16B* siRNA knockdown (40.9 ± 10.3% decrease, n = 3) also significantly reduced the Cl_{Ca} current amplitude (I_{peak} = 39.0 ± 5.5 pA/pF, n = 5, p = 0.0066 *versus* control siRNA; I_{tail} = 31.1 ± 3.3 pA/pF, p = 0.0015) and, in contrast to *Tmem16A* siRNA, increased τ_{act} and τ_{tail} values (τ_{act} = 227.5 ± 6.9 ms, n = 5, p = 0.0003 *versus* control siRNA; τ_{tail} = 158.8 ± 6.8 ms, p = 0.026).

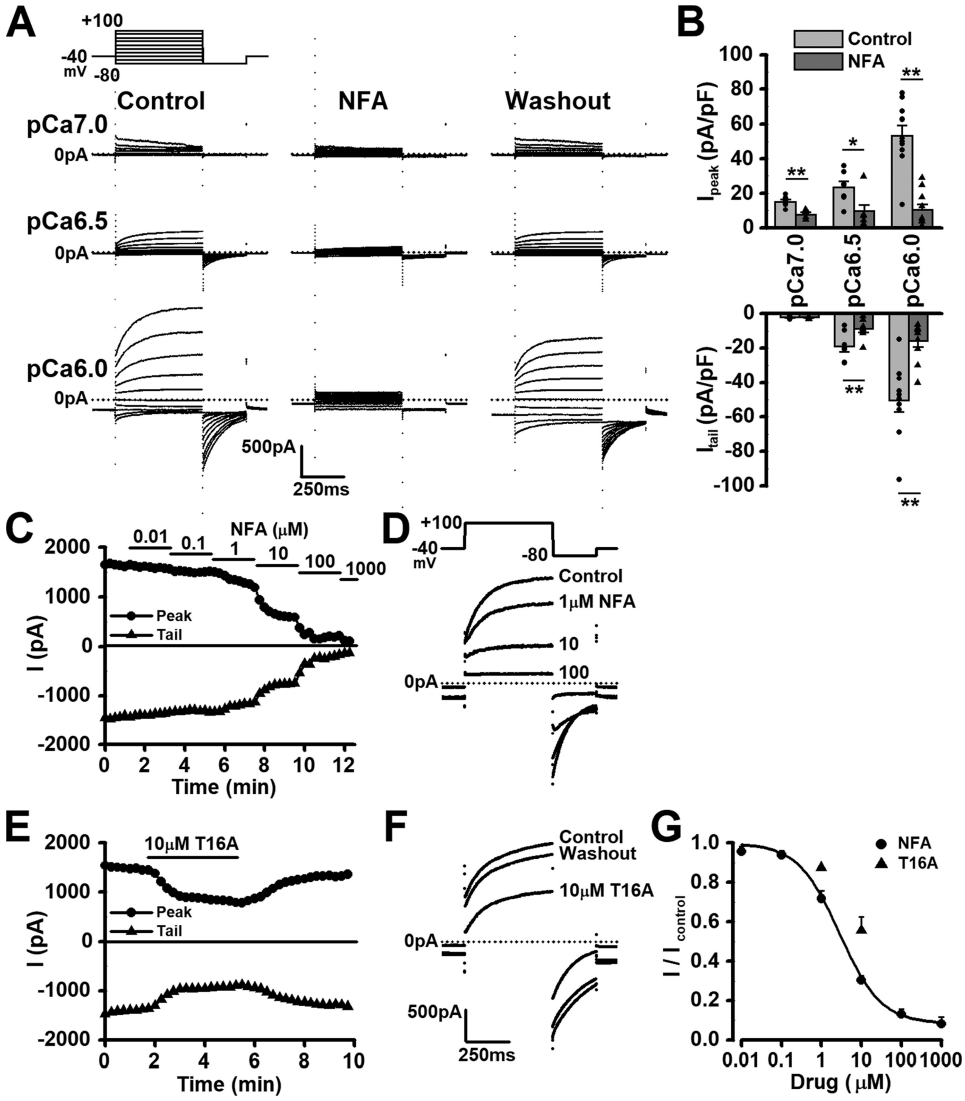

Figure 3. Sensitivity to Cl_{Ca} channel blockers on Cl^- currents in pinealocytes. *A,* under whole-cell voltage-clamp configuration, single pinealocytes were depolarized from the holding potential of −40 mV to test potentials (−80 ~ +100 mV) by +20 mV increment for 500 ms and subsequently repolarized to −80 mV for 250 ms every 15 s. Representative current traces of *p*Ca 7.0, 6.5, and 6.0 in the pipette solution in the absence of drug (*Control*). Application of 100 μM niflumic acid (*NFA*) was inhibited outward and tail currents. The inhibitory effects of niflumic acid were removed by washout. *B,* effect of 100 μM niflumic acid on outward currents at +100 mV and tail currents at −80 mV following +100 mV depolarization. *C,* time course showing a dose-dependent inhibition of niflumic acid (0.01~1000 μM) on outward (at +100 mV; peak) and tail (at −80 mV following +100 mV depolarization) currents at *p*Ca 6.0 in the pipette solution. *D,* representative current traces in the absence and presence of 1, 10, and 100 μM niflumic acid. *E,* time course showing an inhibitory effect of 10 μM $T16A_{inh}$-A01 (*T16A*) on outward and tail currents. *F,* representative current traces in the absence and presence of 10 μM $T16A_{inh}$-A01. The inhibitory effect of $T16A_{inh}$-A01 was removed by washout. *G,* dose-response curves for niflumic acid and $T16A_{inh}$-A01 on outward currents. The IC_{50} value of niflumic acid was 2.6 μM and the Hill coefficient of 0.81. $T16A_{inh}$-A01 also blocked outward currents in a concentration-dependent manner. Experimental data were obtained from 3 to 10 pinealocytes. *, $p < 0.05$; **, $p < 0.01$ by Student's *t* test (paired).

Furthermore, double siRNA knockdown (*Tmem16A*, 80.3 ± 17.8% decrease, $n = 3$; *Tmem16B*, 46.3 ± 13.3% decrease, $n = 3$) caused almost complete suppression of Cl_{Ca} currents (I_{peak} = 14.0 ± 1.4 pA/pF, $n = 7$, $p = 0.000003$ *versus Tmem16A* siRNA alone, $p = 0.0048$ *versus Tmem16B* siRNA alone; I_{tail} = 11.9 ± 1.7 pA/pF, $p = 0.0002$ *versus Tmem16A* siRNA alone, $p = 0.0031$ *versus Tmem16B* siRNA alone). These results strongly suggest that pineal Cl_{Ca} channels are composed of TMEM16A- and TMEM16B-coding proteins.

TMEM16A and TMEM16B currents in HEK293 cells

To obtain new information concerning the comparative contributions of TMEM16A and TMEM16B to Cl_{Ca} currents in pinealocytes, the electrophysiological parameters of cloned rat TMEM16A and TMEM16B channels were measured in HEK293 cells, in which heterologous expression was performed. In TMEM16A-transfected HEK293 cells, outward and tail currents were not detected, when $[Ca^{2+}]_{pip}$ was *p*Ca 7.0 ($n = 3$), but were consistently observed in a concentration-dependent manner at *p*Ca 6.5 (I_{peak} = 28.3 ± 7.2 pA/pF and I_{tail} = 16.6 ± 5.3 pA/pF, $n = 5$) and 6.0 (81.5 ± 28.6 and 63.6 ± 18.9 pA/pF, respectively, $n = 5$) (Fig. 7, *A*, *B*, and *G*). In contrast, in TMEM16B-transfected cells, these currents were not detected at *p*Ca 7.0 and 6.5 ($n = 4$), and observed at *p*Ca 6.0 (I_{peak} = 65.9 ± 4.6 pA/pF and I_{tail} = 24.5 ± 3.8 pA/pF, $n = 4$) (Fig. 7, *C*, *D*, and *G*). When TMEM16A and TMEM16B cDNAs were co-

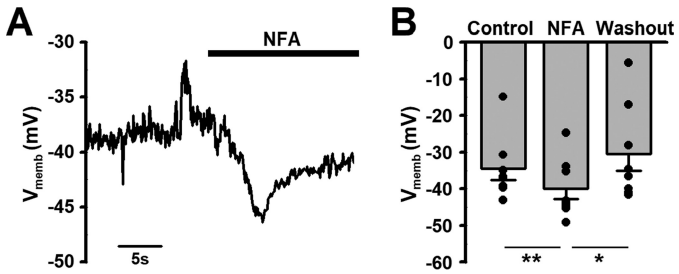

Figure 4. Effect of Cl_{Ca} channel blocker on resting membrane potential in pinealocytes. *A,* a representative trace of membrane potential in single pinealocyte under current-clamp mode. Note that blockade of Cl_{Ca} channels by 100 μM niflumic acid (*NFA*) caused a membrane hyperpolarization. *B,* effect of niflumic acid on the resting membrane potential. Experimental data were obtained from 8 pinealocytes. *, $p < 0.05$; **, $p < 0.01$ by Student's *t* test (paired).

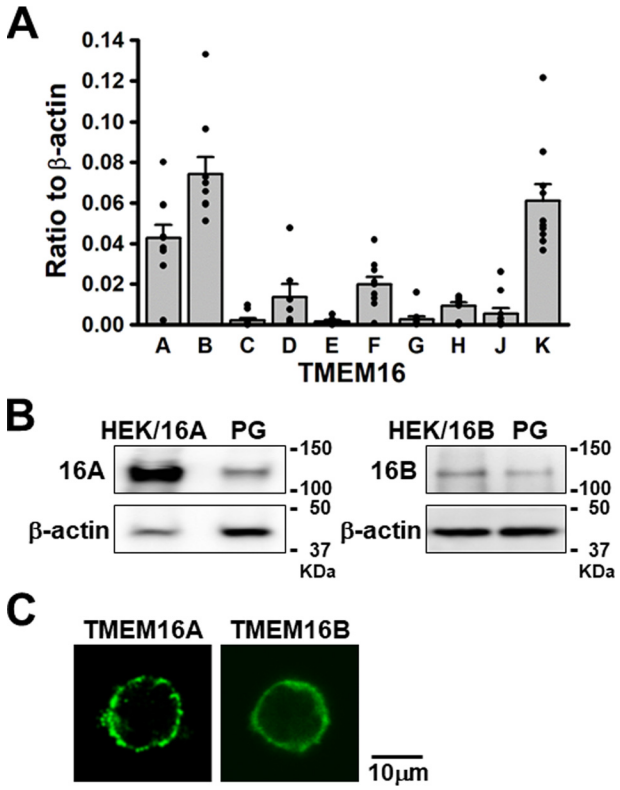

Figure 5. Expression analysis of TMEM16 family in rat pineal glands. *A,* quantitative real-time PCR analysis. Note that mRNA expressions of *Tmem16A* and *Tmem16B* are abundant in rat pineal glands ($n = 10$ experiments). *B,* Western blot analysis of TMEM16A and TMEM16B using the plasma membrane fraction from pineal glands (*PG*). Membrane protein extract from HEK293 cells transiently expressed with rat TMEM16A or TMEM16B cDNA was loaded as a positive control. Content of loading protein (10~40 μg/lane) was confirmed by β-actin ($n = 6–8$ experiments). *C,* immunocytochemical staining of TMEM16A and TMEM16B proteins in pinealocytes. Note that TMEM16A and TMEM16B proteins were expressed in the plasma membrane of pinealocytes ($n = 10$ cells).

transfected at a ratio of 1:2 into HEK293 cells, these currents were recorded at *p*Ca 6.5 ($I_{peak} = 17.3 \pm 1.4$ pA/pF and $I_{tail} = 15.3 \pm 1.7$ pA/pF, $n = 4$) and 6.0 (99.6 ± 15.8 and 70.5 ± 2.2 pA/pF, respectively, $n = 4$) (Fig. 7, *E–G*). Interestingly, in TMEM16A/B-cotransfected cells at ratios of 1:1 or 1:2, the τ_{act} and τ_{tail} values at a 1:2 ratio (108.9 ± 20.4 and 86.5 ± 5.2 ms, respectively, $n = 4$) were closer to these of pineal Cl_{Ca} currents (80.5 ± 8.4 and 81.0 ± 8.9 ms, respectively, $n = 8$) than those at 1:1 (150.2 ± 18.7 and 106.1 ± 14.7 ms, respectively, $n = 4$) (Fig. 7, *H* and *I*). Furthermore, the TMEM16B–TMEM16A tandem form was also transfected into HEK293 cells. Cl_{Ca}-like currents recorded in tandem-transfected cells at *p*Ca 6.0 ($I_{peak} = 66.8 \pm 19.4$ pA/pF and $I_{tail} = 39.3 \pm 13.5$ pA/pF, $n = 5$) and the parameters ($\tau_{act} = 185.0 \pm 26.3$ ms and $\tau_{tail} = 89.6 \pm 6.3$ ms) were close to co-transfection at a 1:1 ratio. The result indicates that both TMEM16A and TMEM16B are functionally expressed and responsible for pineal Cl_{Ca} currents.

Molecular interaction between TMEM16A and TMEM16B in living HEK293 cells

Although it has been reported that the TMEM16 family can form heterodimers mainly based on co-immunoprecipitation assays using a heterologous expression system (21), little is known about this interaction in living cells. Bimolecular fluorescent complementation (BiFC) analysis can detect a direct interaction between two molecules fused, respectively, with the N or C terminus of Venus (VN173 or VC155) by the generation of reconstructed Venus fluorescence (22–24). As shown in Fig. 8, the strong fluorescent signals of Venus were observed at the plasma membrane in homomeric TMEM16A-VN/TMEM16A-VC and TMEM16B-VN/TMEM16B-VC co-expressing HEK293 cells ($n = 10$) (Fig. 8, *A* and *B*). Similarly, the consistent Venus signals in heteromeric TMEM16A-VN/TMEM16B-VC and TMEM16A-VC/TMEM16B-VN HEK293 cells were detected at the plasma membrane ($n = 10$) (Fig. 8*C*). In contrast, there were no fluorescent signals in HEK293 cells expressing TMEM16A-VN, TMEM16B-VN, TMEM16A-VC, or TMEM16B-VC alone ($n = 10$). In addition, fluorescent signals were not detected in HEK293 cells co-expressing TMEM16A-VC/TASK1-VN or TMEM16B-VC/TASK1-VN ($n = 10$) (Fig. 8*D*). These data support that TMEM16A directly interacts with TMEM16B to form a heteromeric in addition to homomeric channels in living cells.

Homo- and heteromeric TMEM16A and TMEM16B channels in living HEK293 cells

To confirm the formation and examine its efficiency of homo- or heterodimer of TMEM16A and TMEM16B, FRET analyses with a total internal reflection fluorescence (TIRF) microscope at the single molecule level were performed in HEK293 cells, as reported previously (22–28). These single molecule images revealed that a subset of YFP-TMEM16A fluorescent signals overlapped with TMEM16B-CFP signals, and that the proportion of co-localization was 50.1 ± 5.4% ($n = 5$) (Fig. 9, *A* and *B*). On the other hand, the co-localization proportion of YFP-TMEM16B and TMEM16B-CFP was 60.7 ± 5.8% ($n = 5$). Thereafter, the YFP signal was photobleached to less than 30% of the control. In YFP-TMEM16A/TMEM16B-CFP co-expressing HEK293 cells, the fluorescent intensity of CFP was significantly enhanced after photobleaching (efficiency of FRET, $E_{FRET} = 10.0 \pm 1.0$%, 26 particles from 5 cells, $p = 0.00008$ ($F = 25.49$) *versus* −0.5 ± 1.2% of TMEM16B-CFP alone, 28 particles from 5 cells, by Tukey's test) (Fig. 9*C*). The E_{FRET} value in YFP-TMEM16B/TMEM16B-CFP HEK293 cells was 15.7 ± 2.3% (29 particles from 5 cells, $p = 0.000001$). This TIRF-FRET analysis suggests that TMEM16A and TMEM16B

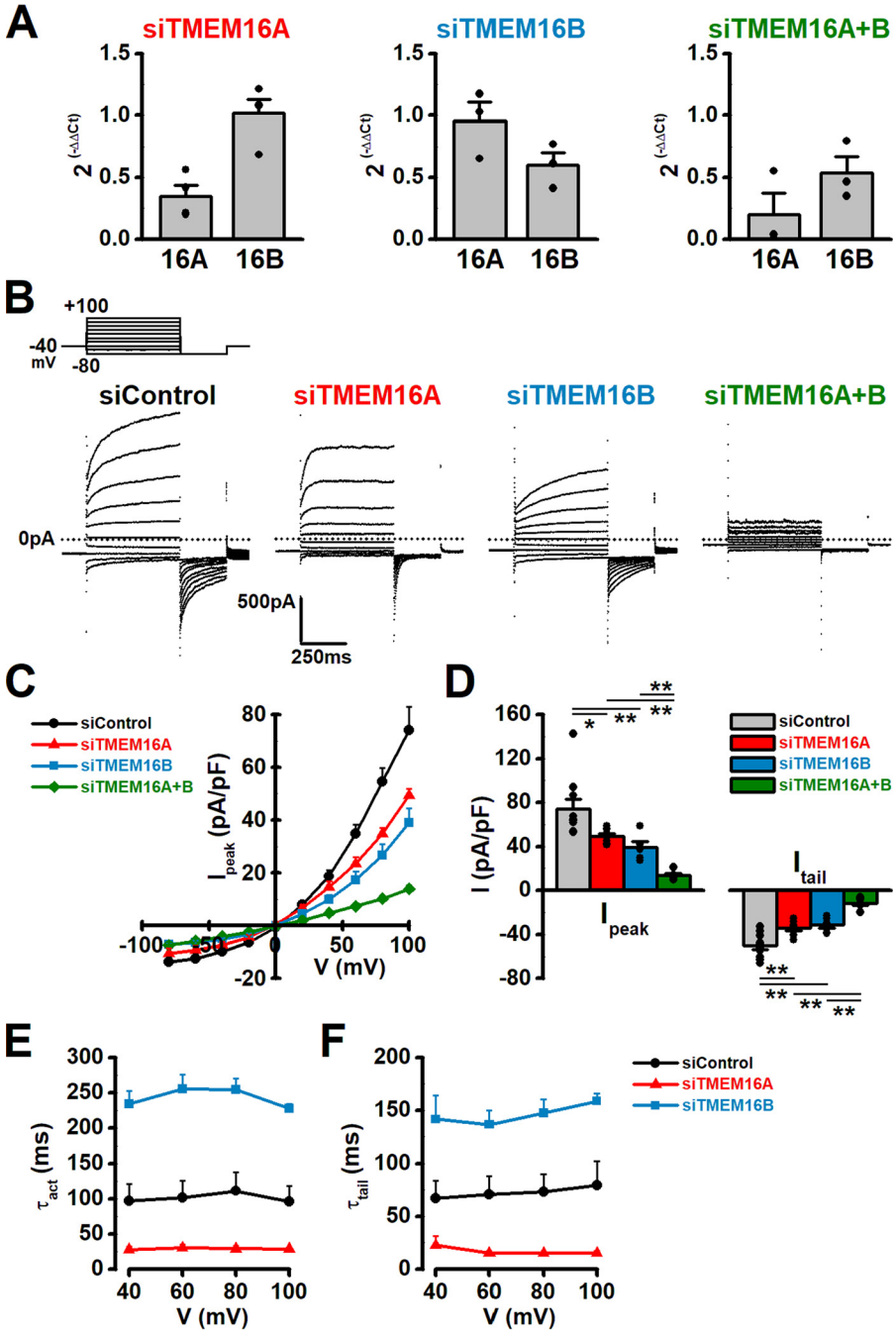

Figure 6. Pineal Cl_{Ca} currents formed by TMEM16A and TMEM16B. *A,* knockdown efficiency by *Tmem16A* and *Tmem16B* siRNAs in rat pinealocytes. The selectivity of *Tmem16A* and *Tmem16B* siRNAs was confirmed by a quantitative real-time PCR method. Expression efficiency of *Tmem16A* and/or *Tmem16B* siRNAs was normalized by control siRNA (*siControl*). Note that *Tmem16A* and *Tmem16B* siRNAs can selectively knockdown corresponding mRNA ($n = 3{\sim}4$ experiments). *B,* single pinealocytes were depolarized from the holding potential of −40 mV to test potentials (−80 ∼ +100 mV) by +20 mV increment for 500 ms and subsequently repolarized to −80 mV for 250 ms every 15 s. Representative current traces of Cl_{Ca} currents in rat pinealocytes transfected with control, *Tmem16A*, *Tmem16B*, or *Tmem16A* + *Tmem16B* siRNA. *C,* current-voltage relationships of outward currents in pinealocytes transfected with control, *Tmem16A*, *Tmem16B*, or *Tmem16A* + *Tmem16B* siRNA. *D,* outward (at +100 mV: peak) and tail (at −80 mV following +100 mV depolarization) current densities. *E,* τ_{act} of outward currents. *F,* τ_{tail} of tail currents. Experimental data were obtained from 5 to 10 pinealocytes. *, $p < 0.05$; **, $p < 0.01$ by Tukey's test.

can form heteromeric channels with efficiency comparative to that of homomeric channels.

Evidence for heteromeric TMEM16A/B channels in pineal glands

To our knowledge, there is no report showing the heteromeric channel formation of TMEM16A and TMEM16B in native tissues. As shown in Fig. 10, our co-immunoprecipitation results demonstrate heteromeric interaction of TMEM16A and TMEM16B in rat pineal glands ($n = 4$).

Discussion

The pineal gland is a melatonin-secreting organ in the brain. It regulates circadian rhythm through the synthesis and secretion of melatonin. This regulation of melatonin production depends upon a balance of activity, modulated by sympathetic

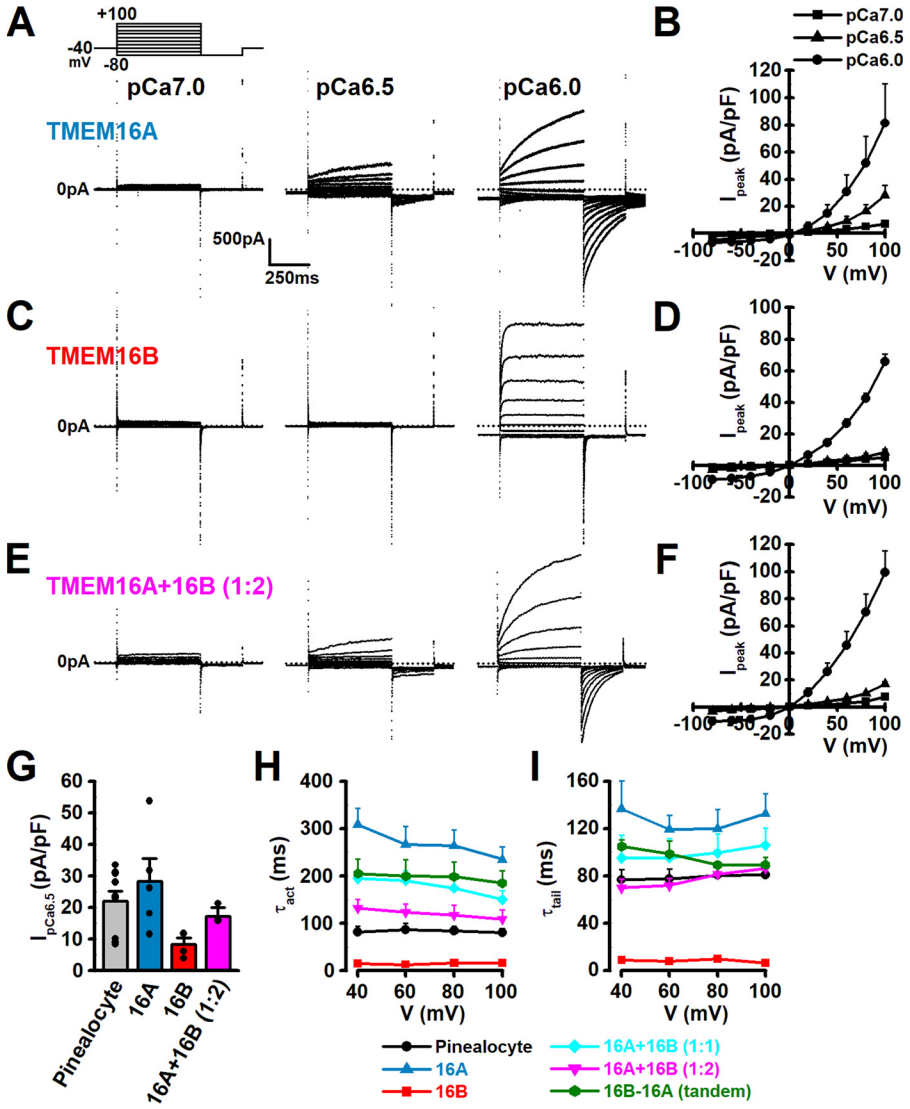

Figure 7. Current properties of TMEM16A and TMEM16B cloned from rat pinealocytes. *A–F*, rat TMEM16A (3 μg), TMEM16B (3 μg), or TMEM16A + TMEM16B (1 + 2 μg) cDNA was transfected into HEK293 cells. HEK293 cells were depolarized from the holding potential of −40 mV to test potentials (−80 ~ +100 mV) by +20 mV increment for 500 ms and subsequently repolarized to −80 mV for 250 ms every 15 s. Representative traces of Cl_{Ca} currents and their current-voltage relationships at *p*Ca 7.0, 6.5, and 6.0 in the pipette solution from HEK293 cells expressing TMEM16A (*A* and *B*), TMEM16B (*C* and *D*), or TMEM16A + TMEM16B (*E* and *F*). *G*, outward current density at +100 mV at *p*Ca 6.5. *H*, τ_{act} of outward currents in pinealocytes and HEK293 cells transfected with TMEM16A, TMEM16B, TMEM16A + TMEM16B (1:1), TMEM16A + TMEM16B (1:2), or TMEM16B–TMEM16A tandem form. *I*, τ_{tail} of tail currents. Note that the predominant electrophysiological properties of pinealocytes are very similar to these of TMEM16A/TMEM16B (1:2) co-expressing HEK293 cells. Data from pinealocytes have been replotted from Fig. 2. Experimental data were obtained from 4 to 8 cells.

and parasympathetic innervation (1, 2). Although meaningful electrophysiological studies have been done, no comprehensive analyses of the functional expressions of ion channels has been reported in mammalian pineal glands. Accordingly, the physiological roles of specific ion channels in the regulation of melatonin secretion are not known. Our new results show that TMEM16A and TMEM16B proteins are the predominant Cl_{Ca} channel subtype in pinealocytes, and demonstrate that this Cl^- conductance is involved in melatonin secretion in pineal glands.

In rat pinealocytes, substantial voltage-dependent Cl^- currents have been recorded by a whole-cell patch clamp technique, after K^+ currents were totally blocked by Cs^+ and tetraethylammonium. Depolarizing voltage steps to positive membrane potentials elicited a slow time-dependent outward current; and subsequent repolarization produced a characteristic inward tail current. The amplitude of these currents was highly dependent on $[Ca^{2+}]_i$ in the range of *p*Ca 7.0~6.0 in the pipette solution. This current reversed near 0 mV, which is a theoretical equilibrium potential of Cl^- ($E_{Cl} = -0.9$ mV) under our experimental conditions. Furthermore, these currents were strongly inhibited by a specific blocker of TMEM16A and TMEM16B channels, $T16A_{inh}$-A01, as well as a classical Cl_{Ca} channel blocker, niflumic acid. To our knowledge, this is first demonstration of Cl_{Ca} current in pineal glands.

Cl_{Ca} channels are ubiquitously expressed in epithelia, smooth muscles, interstitial cells of Cajal, and some neurons (18–20). In neurons and smooth muscles, an increase in Cl_{Ca} conductance significantly shifts the resting membrane potential in the depolarizing direction. This facilitates Ca^{2+} influx

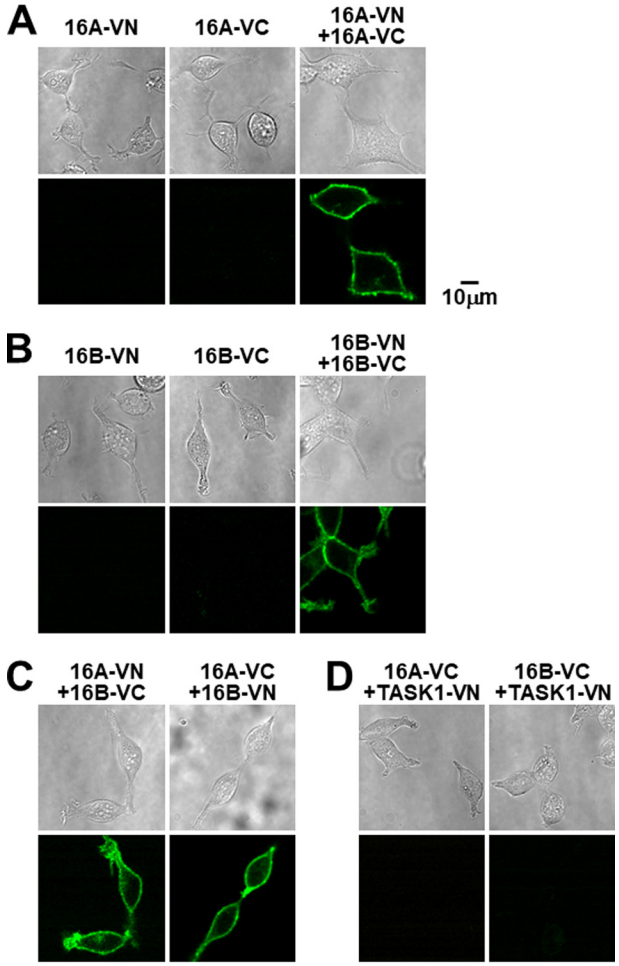

Figure 8. Molecular interaction between TMEM16A and TMEM16B. *A* and *B,* representative transmitted and fluorescent confocal images of HEK293 cells transfected with TMEM16A (*A*) or TMEM16B (*B*) fused with fluorescent fraction of the Venus protein (VN173 or VC155) in a BiFC assay. *C,* representative confocal images of HEK293 cells co-transfected with TMEM16A-VN/TMEM16B-VC or TMEM16A-VC/TMEM16B-VN in BiFC assay. Note that fluorescent signals of Venus were detected in heteromeric TMEM16A/TMEM16B cells, as well as homomeric TMEM16A and TMEM16B cells. *D,* representative BiFC images of TMEM16A-VC/TASK1-VN or TMEM16B-VC/TASK1-VN co-expressing HEK293 cells. Experimental data were obtained from 10 cells.

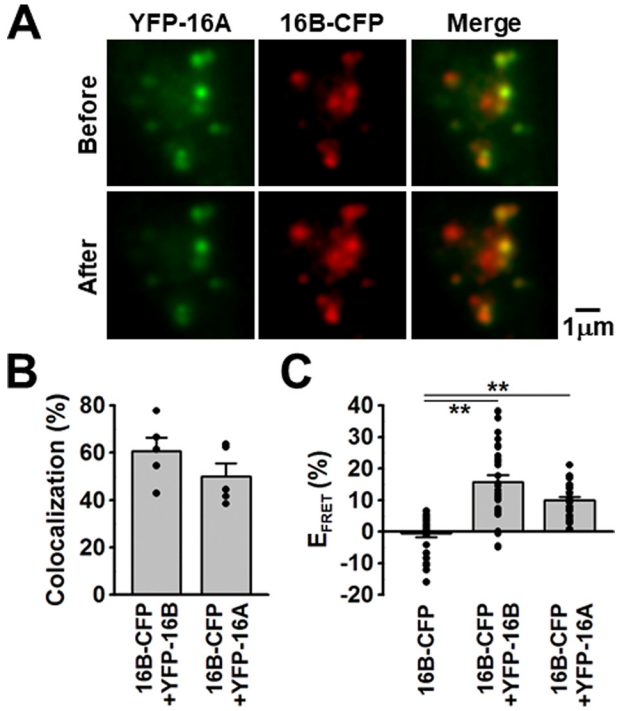

Figure 9. Single-molecule imaging of TMEM16A and TMEM16B. *A,* YFP-TMEM16A (acceptor) and TMEM16B-CFP (donor) were transiently co-transfected into HEK293 cells. Single-molecule images were obtained by TIRF microscopy. Note that CFP fluorescent signals were enhanced after YFP photobleaching. *B,* co-localization rate of CFP and YFP fluorescent signals in TMEM16B-CFP/YFP-TMEM16B or TMEM16B-CFP/YFP-TMEM16A HEK293 cells ($n = 5$ cells). *C,* E_{FRET} of TMEM16B-CFP alone (as a negative control), TMEM16B-CFP/YFP-TMEM16B (as a positive control), or TMEM16B-CFP/YFP-TMEM16A HEK293 cells ($n = 26\sim29$ particles from 5 cells). **, $p < 0.01$ by Tukey's test.

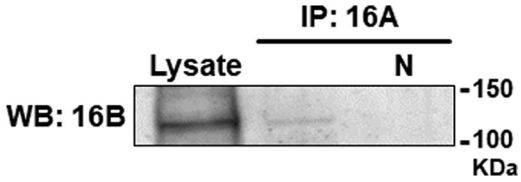

Figure 10. Co-immunoprecipitation assay for TMEM16A and TMEM16B in rat pineal glands. In co-immunoprecipitation assays, lysates from rat pineal glands were precipitated with TMEM16A antibody and blotted using TMEM16B antibody. *N* indicates a negative control lane loaded with protein treated with the Control Agarose Resin (see "Experimental procedures"). Similar results were obtained from four independent experiments.

through VDCCs, resulting in the enhancement of cell excitability in the form of Ca^{2+}-dependent action potentials. TMEM16A and TMEM16B are currently the preferred candidates for Cl_{Ca} channel conductances in native tissues. Specifically, among neurons, TMEM16A is expressed in small dorsal root ganglion neurons associated with nociception (29) and thermoreceptors (30). On the other hand, TMEM16B is expressed in presynaptic terminals of retinal photoreceptors (31) and the cilia of olfactory sensory neurons (32, 33), where it appears to play a special role in sensory transduction. In addition, TMEM16B can regulate action potential waveform, and synaptic responses in hippocampus neurons (34). Our results demonstrate that both TMEM16A and TMEM16B proteins are abundantly expressed at the plasma membrane of rat pinealocytes. Although the *Tmem16K* transcript was also expressed in pinealocytes, it is rather unlikely that TMEM16K *per se* forms a functional Cl_{Ca} channel (20). Therefore, the present study focused on physiological functions of TMEM16A and TMEM16B in pinealocytes.

The biophysical characteristics of TMEM16B channels show significant differences from those of TMEM16A channels. First, the single-channel conductance of the TMEM16B channel (0.8∼1.2 pS) has been reported to be smaller than that of the TMEM16A channel (8.3 pS) (17, 32, 35). However, a recent report suggests that there are no significant differences between both channels (TMEM16A = 3.5 pS *versus* TMEM16B = 3.9 pS) (36). Second, the $[Ca^{2+}]_i$ level needed for activation of the TMEM16B channel (>1 μM) is higher than that of the TMEM16A channel (∼0.3 μM) (17, 32, 36–38). Third, the kinetics of activation and deactivation (τ_{deact}) of the TMEM16B current are much faster than those of the TMEM16A current. The τ_{act} and τ_{deact} of TMEM16B are 4–24 at +100 mV and 3–7 ms at −60 ∼ −100 mV, respectively (35, 36, 38). In contrast, those of TMEM16A are ranged between 120∼400 and 55∼150 ms, respectively (36, 38, 39). In the pres-

ent study, pineal Cl_{Ca} currents were significantly activated by 0.3 μM $[Ca^{2+}]_i$, which suggests TMEM16A involvement. The kinetic parameters of pineal Cl_{Ca} currents were intermediate with respect to those of TMEM16A and TMEM16B.

In addition, siRNA experiments revealed that treatment with either siTMEM16A or siTMEM16B resulted in the remaining much smaller Cl_{Ca} current having characteristics of the remaining TMEM16A/B channels. As expected, therefore, pineal Cl_{Ca} currents were completely abolished by double siRNA knockdown of *Tmem16A* and *Tmem16B*. In separate experiments, the most prominent biophysical properties of pineal Cl_{Ca} currents were mimicked by HEK293 cells that co-expressed TMEM16A and TMEM16B, which were cloned from rat pineal glands. A proportion of 1:2 for TMEM16A and TMEM16B co-transfection to HEK293 cells was determined based on the mRNA expression level in rat pineal glands. This 1:2 expression ratio rather than 1:1 resulted in the functional expression of the more closely mimicked Cl_{Ca} current with respect to kinetics parameters to those of native Cl_{Ca} current in rat pinealocytes. In combination, these results strongly suggest that both of TMEM16A and TMEM16B functionally contribute to Cl_{Ca} current in pinealocytes.

It is known that the expression pattern of TMEM16A proteins is distinct from that of TMEM16B proteins; therefore, each protein is presumed to form a homodimer as a functional Cl_{Ca} channel in native cells (27, 40, 41). In heterologous expression systems, TMEM16A protein can interact with TMEM16B protein, resulting in heterodimeric channels (21). Therefore, TMEM16A and TMEM16B heterodimers may form in native cells co-expressing both proteins. The expression of both proteins has been reported in rodent tissues, but the expression patterns are different; TMEM16A is found mainly in secretory epithelia *versus* TMEM16B in chemosensory neurons (42). In murine olfactory epithelium, the TMEM16A channel regulates Cl^- homeostasis in supporting cells, whereas the TMEM16B channel contributes to the olfactory signal transduction in sensory neurons (43). Although TMEM16A and TMEM16B proteins are expressed in mammalian uterine smooth muscles (44) and dorsal root ganglion (45), heteromeric channel formation has not been demonstrated. Our results show that, in rat pinealocytes, TMEM16A and TMEM16B were co-expressed and that these proteins can form heteromeric assembly as well as homomeric channels. The heteromeric formation in living cells was clearly detected by BiFC analyses in HEK293 cells. The results of FRET analyses suggest that the efficiency of heterodimerization appears to be comparative to those of homodimerization. In addition, Cl_{Ca} currents were observed in HEK293 cells transfected with the TMEM16B–TMEM16A tandem form. Taken together, it appears that pineal Cl_{Ca} channels are composed of heteromeric TMEM16A and TMEM16B complexes, in addition to homomers.

Melatonin assays revealed that Cl_{Ca} channel blockers can reduce the NE-induced melatonin secretion. The intracellular Cl^- concentration varies widely, 10–60 mM, depending on tissues (46). Although the intracellular Cl^- concentration in pinealocytes is not known, Cl_{Ca} channel block caused a consistent hyperpolarization under our experimental conditions, where the equilibrium potential of Cl^- was set at 0 mV. Under physiological conditions, the equilibrium potential of Cl^- in pinealocytes may be between −20 and −70 mV. Taken together, when action potentials occur spontaneously (5–9) or in response to endogenous stimulation, Cl_{Ca} channel activation by Ca^{2+} influx may increase the repolarization current and reduce the action potential duration. Further experiments are necessary for elucidating the molecular mechanism underlying the modulation of melatonin secretion by Cl_{Ca} channel activity.

In conclusion, pineal Cl_{Ca} currents flow through homomeric and heteromeric channels based on TMEM16A and TMEM16B subunits. The functional activity of Cl_{Ca} channels significantly contributes to the regulation of melatonin secretion. Thus this study provides novel information concerning the molecular mechanism that regulates circadian rhythm through melatonin secretion in pineal glands.

Experimental procedures

Ethical approval

All experiments were approved by the Ethics Committee of Nagoya City University and were conducted in accordance with the Guide for the Care and Use of Laboratory Animals of the Japanese Pharmacological Society.

Melatonin assay

Pineal glands were removed from male Wistar/ST rats (6∼9 weeks; Japan SLC, Hamamatsu, Japan). The freshly dissected pineal glands were incubated for 1 h at 37 °C in phosphate-buffered saline (PBS) and then exposed to 1 μM NE or vehicle (control) for 2 h. Test compounds were added into PBS at the beginning of incubation prior to NE addition. The amount of melatonin secreted from the whole pineal gland was quantitatively determined using a melatonin ELISA kit (IBL International, Hamburg, Germany).

Cell culture

Pineal glands were incubated in PBS containing 0.1% collagenase (Wako Pure Chemical Industries, Osaka, Japan) and 0.02% trypsin (Type I; Sigma) for 25 min at 37 °C (9). After incubation, these tissues were dispersed mechanically in PBS. The pinealocytes were cultured on coverslips coated with 5 μg/ml of poly-L-lysine (Sigma) in Dulbecco's modified Eagle's medium supplemented with 10% heat-inactivated fetal bovine serum (Invitrogen/Gibco), 20 units/ml of penicillin, and 20 μg/ml of streptomycin (Wako Pure Chemical Industries). Experiments were performed at 24∼96 h after cell culture.

Electrophysiological recording

Electrophysiological studies were carried out using a whole-cell patch clamp technique with a CEZ-2400 (Nihon Kohden, Tokyo, Japan) amplifier, an analog digital converter (Digidata 1440A; Molecular Devices/Axon, Foster City, CA), and pCLAMP software (version 10; Molecular Devices/Axon) in single pinealocytes and HEK293 cells (25, 47). The pipette resistance ranged from 3 to 5 MΩ when filled with the pipette solution. The seal resistance was ∼30 GΩ. Series resistance was between 5 and 8 MΩ and was partly compensated. Under whole-cell voltage-clamp mode, cells were step-clamed from

the holding potential of −40 mV to test potentials (−80 ∼ +100 mV) by +20 mV increment for 500 ms and subsequently returned to −80 mV for 250 ms every 15 s. Electrophysiological data were acquired at 1 kHz. The HEPES-buffered solution was used as an extracellular solution: 137 mM NaCl, 5.9 mM KCl, 2.2 mM $CaCl_2$, 1.2 mM $MgCl_2$, 14 mM glucose, and 10 mM HEPES. The pH was adjusted to 7.4 with 10 N NaOH. The pipette solution for Cl_{Ca} current measurement had the following ionic composition: 120 mM CsCl, 20 mM tetraethylammonium-Cl, 2.8 mM $MgCl_2$, 2 mM $ATPNa_2$, 10 mM HEPES, 5 mM EGTA, and 1.79 (*p*Ca 7.0), 3.19 (*p*Ca 6.5), or 4.25 mM (*p*Ca 6.0) $CaCl_2$. The pH was adjusted to 7.2 with 1 N CsOH. For the recording of membrane potential under whole-cell current-clamp mode, the pipette solution had the following ionic composition: 140 mM KCl, 4 mM $MgCl_2$, 2 mM $ATPNa_2$, 10 mM HEPES, and 0.05 mM EGTA. The pH was adjusted to 7.2 with 1 N KOH. Electrophysiological recordings were performed at room temperature (23–25 °C).

Quantitative real-time PCR

The total RNA extraction from homogenates of rat pineal glands, the reverse transcription method, and quantitative real-time PCR analysis using ABI PRISM 7000 sequence detection system (Applied Biosystems, Foster City, CA) and LightCycler 96 real-time PCR system (Roche Diagnostics, Mannheim, Germany), were performed as reported previously (9). Specific primers for rat TMEM16 genes were designed as follows: *Tmem16A* (GenBank™ accession number, NM_001107564), (+) GGG AGA AGC AAC ACT TAT TCG A, (−) TGC ACG TTG TTC TCT TCA GGA T; *Tmem16B* (XM_003753944), (+) GGG ACC TGA CTG GGA TAG AAG, (−) GCC ACT CTC CTT TAG CAG TTT C; *Tmem16C* (XM_230381), (+) TCC TAG CGG CTG TCT GAT AGA, (−) GAC CAC CAG TTT TGG ATT AAC G; *Tmem16D* (NM_001106778), (+) GTC CGT GTT CCG AAT TTC TGA, (−) AGT CCC GAT ATC TGC AGT ACT TCA; *Tmem16E* (NM_003753253), (+) CAT CGC ATC CCC TGG TAC TTT, (−) ACT GAT AGG CGG TAC ACG ATA ATG; *Tmem16F* (NM_001108108), (+) GTG GAT GCG TGG AAG CTT ACA, (−) AGG ATG GCT ATT CCT TGC ATG A; *Tmem16G* (NM_001004071), (+) TGG CTT GGG TTC TAC ACT GGT T, (−) TGC GTT GGT ACA TCT GAG AAC A; *Tmem16H* (XM_002728392), (+) AGA GCA CTT GGC TCT TCT AGT CA, (−) GTC GCT GGT ACT CCA ATT TGG; *Tmem16J* (XM_001062059), (+) CTC TCA GAG ATG TGC ACT TTT GC, (−) AGG AAG ACC GTA GCC CAC AGA; *Tmem16K* (XM_236774), (+) AGA AGG AAA TGG GCA CTT ACC T, (−) TGC TAA CGG GTA AAC GCA AGA; and β-actin (NM_031144), (+) AGG CCA ACC GTG AAA AGA TG, (−) ACC AGA GGC ATA CAG GGA CA.

Western blotting

Western blotting experiments were performed as described previously (48). In brief, the protein fraction of plasma membrane was extracted from rat pineal glands, and 10–40 μg/lane of protein was subjected to 7.5% SDS-PAGE. The resulting blots were incubated with TMEM16A (1:100 dilution; ab53212, Abcam, Cambridge, MA) or TMEM16B (1:200 dilution; ab91573, Abcam) antibody for 12 h at 4 °C, and then treated with anti-rabbit horseradish peroxidase-conjugated IgG (1:2000 dilution; Chemicon International, Temecula, CA) for 1 h at 4 °C, and finally exposed to an enhanced chemiluminescence detection system (Amersham Biosciences). For quantitative analyses, β-actin antibody (1:5000 dilution; A1978, Sigma) and anti-mouse horseradish peroxidase-conjugated IgG (1:2000 dilution; Chemicon International) were used. The luminescence images were analyzed using a LAS-3000 system (Fujifilm, Tokyo, Japan).

Immunocytochemistry

Immunocytochemical staining was performed as reported previously (9). In brief, freshly isolated rat pinealocytes were fixed with 4% paraformaldehyde in PBS for 10 min at room temperature. These pinealocytes were treated with TMEM16A (1:100 dilution) or TMEM16B (1:100 dilution) antibody for 12 h at 4 °C, and then covered with Alexa Fluor 488-labeled secondary antibody solution (1:1000 dilution; A11008, Invitrogen/Molecular Probes) for 1 h at room temperature. Confocal images were obtained using a laser scanning confocal fluorescent microscope (A1R; Nikon, Tokyo, Japan).

siRNA knockdown

Knockdown of *Tmem16A* and/or *Tmem16B* was performed using the siRNA method. Control (Medium GC Duplex #3), *Tmem16A* (Stealth RNAi, Tmem16aRSS317801), and *Tmem16B* (LOC683001RSS369708) siRNAs were obtained from Invitrogen. At 4 h after enzymatic cell isolation, pinealocytes were transfected with 67 nM siRNA construct plus the BLOCK-iT Fluorescent Oligo (Invitrogen) as an expression marker using Lipofectamine RNAiMAX reagent (Invitrogen). Experiments were performed 24–68 h after transfection.

Molecular cloning

The cDNAs encoding *Tmem16A* and *Tmem16B* were cloned from rat pineal glands using specific PCR primers: *Tmem16A* (GenBank™ accession number, XM_006230780), (+) cacc ggtacc gcc gcc acc ATG CAG GAC ACA CAG GAC AGC GA, (−) cacc ctcgag CTA CAG CGC GCC CCC ATG GTA CTC GTA GCT; and *Tmem16B* (XM_003753944), (+) cacc ggtacc gcc gcc acc ATG GCG GCC CCT GGG CTG CAA GAC ATC CCT, (−) cacc gaattc TCA TAC GTT GGT GTG CTG GGA CCC T. Then these full-length cDNAs were subcloned into pcDNA3.1(+)/Neo (Invitrogen), pECFP-N1, pEYFP-C1 (Clontech Laboratories, Mountain View, CA), pBiFC-VN173 (plasmid number 22010, Addgene), and pBiFC-VC155 (number 22011, Addgene) (49) vectors. A tandem form with a $(GGGGS)_3$ linker domain, TMEM16B-(ggt gga ggc ggt tca ggc gga ggt ggc tct ggc ggt ggc gga tcg)-TMEM16A, cDNA were subcloned into pECFP-N1 vector. Finally, the cDNA(s) (total 3 μg) were transiently transfected into HEK293 cells using Lipofectamine 2000 reagent (Invitrogen). Experiments were performed 24–72 h after transfection.

BiFC analysis

The direct molecular interaction between TMEM16A and TMEM16B proteins in live cells was analyzed based on the BiFC method as reported previously (22). In brief, fragments of the N (1–172; VN173) or C (155–238; VC155) terminus of

Venus were fused to the C terminus of TMEM16A or TMEM16B (TMEM16A-VN, TMEM16A-VC, TMEM16B-VN, and TMEM16B-VC). When VN173- and VC155-fused proteins exist within close proximity, *i.e.* within the same channel, VN173 and VC155 fragments are able to complement, resulting in production of blight fluorescence from Venus. HEK293 cells were transfected with plasmids of constructs labeled by VN173 and VC155 at 1 μg each using Lipofectamine 2000 reagent. As negative controls, in addition to HEK293 cells expressing TMEM16A-VN, TMEM16B-VN, TMEM16A-VC, and TMEM16B-VC alone, HEK293 cells co-expressing either TMEM16A-VC or TMEM16B-VC and TASK1 (KCNK3, a two-pore domain K^+ channel) tagged with VN173 (TASK1-VN) (24) were used. BiFC images were obtained using a laser scanning confocal fluorescent microscope (A1R; Nikon).

FRET analysis

Single-molecule imaging was performed with a TIRF imaging system, which consisted of a fluorescent microscope (ECLIPSE TE2000-U; Nikon), an objective lens (CFI Apo TIRF ×60/1.45, oil immersion; Nikon), an EM-CCD camera (C9100–12; Hamamatsu Photonics, Hamamatsu, Japan), and AQUACOSMOS software (version 2.6; Hamamatsu Photonics), as previously reported (25). In brief, cells were fixed with PBS containing 4% paraformaldehyde for 10 min. E_{FRET} was evaluated based on the acceptor photobleaching method. The fluorescence of YFP was photobleached for 2 min. TIRF images were acquired for 4.65 s. E_{FRET} was calculated using the following equation: E_{FRET} (%) = $[(CFP_{after} - CFP_{before})/CFP_{after}] \times 100$, where CFP_{after} and CFP_{before} are CFP emissions after and before YFP photobleaching, respectively.

Co-immunoprecipitation assay

Co-immunoprecipitation was performed using a co-immunoprecipitation kit (Pierce Biotechnology) as reported previously (23). In brief, seven pineal glands were lysed in immunoprecipitation lysis/wash buffer with a protease inhibitor mixture (Sigma). Homogenates were centrifuged (15,000 × *g*, 25 min, 4 °C), and supernatant was precleared with control resin (1 h, 4 °C). Precleared lysates (~100 μg of protein) were incubated with AminoLink Plus Coupling Resin, with which TMEM16A antibody was immobilized for 12 h at 4 °C. As a negative control, Control Agarose Resin, which was composed of the same support material as the AminoLink Plus Coupling Resin but was not amine-reactive, was used. The incubated lysates were finally subjected to 7.5% SDS-PAGE. The blots were incubated with TMEM16B antibody (1:200 dilution) for 12 h at 4 °C, and then treated with anti-rabbit horseradish peroxidase-conjugated IgG (1:2000 dilution) for 1 h at 4 °C, and finally exposed to an enhanced chemiluminescence detection system. The luminescence images were analyzed using a LAS-3000 system.

Drugs

Pharmacological reagents were obtained from Sigma, except for EGTA and HEPES (Dojin, Kumamoto, Japan). All hydrophobic compounds were dissolved in dimethyl sulfoxide at a concentration of 10–1000 mM as a stock solution.

Statistics

Pooled data are shown as the mean ± S.E. Statistical significance between two groups was determined by Student's *t* test. Statistical significance among groups was determined by Tukey's test after one-way analysis of variance.

Author contributions—H. Y. and Y. I. conceptualization; H. Y. and Y. S. resources; H. Y., K. N., and Y. H. data curation; H. Y., K. N., Y. H., and Y. S. formal analysis; H. Y. and Y. I. funding acquisition; H. Y., K. N., and Y. H. investigation; H. Y. and Y. S. methodology; H. Y. writing-original draft; H. Y. and Y. I. project administration; H. Y. and Y. I. writing-review and editing; Y. I. supervision.

Acknowledgment—We express our sincere thanks to Dr. Wayne R. Giles (University of Calgary, Calgary, Canada) for critical reading and editing of this manuscript.

References

1. Simonneaux, V., and Ribelayga, C. (2003) Generation of the melatonin endocrine message in mammals: a review of the complex regulation of melatonin synthesis by norepinephrine, peptides, and other pineal transmitters. *Pharmacol. Rev.* **55,** 325–395 CrossRef Medline
2. Phansuwan-Pujito, P., Møller, M., and Govitrapong, P. (1999) Cholinergic innervation and function in the mammalian pineal gland. *Microsc. Res. Tech.* **46,** 281–295 CrossRef Medline
3. Yamada, H., Ogura, A., Koizumi, S., Yamaguchi, A., and Moriyama, Y. (1998) Acetylcholine triggers L-glutamate exocytosis via nicotinic receptors and inhibits melatonin synthesis in rat pinealocytes. *J. Neurosci.* **18,** 4946–4952 Medline
4. Yamada, H., Yatsushiro, S., Ishio, S., Hayashi, M., Nishi, T., Yamamoto, A., Futai, M., Yamaguchi, A., and Moriyama, Y. (1998) Metabotropic glutamate receptors negatively regulate melatonin synthesis in rat pinealocytes. *J. Neurosci.* **18,** 2056–2062 Medline
5. Reuss, S., and Vollrath, L. (1984) Electrophysiological properties of rat pinealocytes: evidence for circadian and ultradian rhythms. *Exp. Brain Res.* **55,** 455–461 Medline Medline
6. Freschi, J. E., and Parfitt, A. G. (1986) Intracellular recordings from pineal cells in tissue culture: membrane properties and response to norepinephrine. *Brain Res.* **368,** 366–370 CrossRef Medline
7. Aguayo, L. G., and Weight, F. F. (1988) Characterization of membrane currents in dissociated adult rat pineal cells. *J. Physiol.* **405,** 397–419 CrossRef Medline
8. Zemkova, H., Stojilkovic, S. S., and Klein, D. C. (2011) Norepinephrine causes a biphasic change in mammalian pinealocye membrane potential: role of α_{1B}-adrenoreceptors, phospholipase C, and Ca^{2+}. *Endocrinology* **152,** 3842–3851 CrossRef Medline
9. Mizutani, H., Yamamura, H., Muramatsu, M., Kiyota, K., Nishimura, K., Suzuki, Y., Ohya, S., and Imaizumi, Y. (2014) Spontaneous and nicotine-induced Ca^{2+} oscillations mediated by Ca^{2+} influx in rat pinealocytes. *Am. J. Physiol. Cell Physiol.* **306,** C1008–C1016 CrossRef Medline
10. Castellano, A., López-Barneo, J., and Armstrong, C. M. (1989) Potassium currents in dissociated cells of the rat pineal gland. *Pflügers Arch.* **413,** 644–650 Medline Medline
11. Letz, B., Schomerus, C., Maronde, E., Korf, H. W., and Korbmacher, C. (1997) Stimulation of a nicotinic ACh receptor causes depolarization and activation of L-type Ca^{2+} channels in rat pinealocytes. *J. Physiol.* **499,** 329–340 CrossRef Medline
12. Lee, S. Y., Choi, B. H., Hur, E. M., Lee, J. H., Lee, S. J., Lee, C. O., and Kim, K. T. (2006) Norepinephrine activates store-operated Ca^{2+} entry coupled to large-conductance Ca^{2+}-activated K^+ channels in rat pinealocytes. *Am. J. Physiol. Cell Physiol.* **290,** C1060–C1066 Medline
13. Mizutani, H., Yamamura, H., Muramatsu, M., Hagihara, Y., Suzuki, Y., and Imaizumi, Y. (2016) Modulation of Ca^{2+} oscillation and melatonin secretion by BK_{Ca} channel activity in rat pinealocytes. *Am. J. Physiol. Cell Physiol.* **310,** C740–C747 CrossRef Medline

14. Darvish, N., and Russell, J. T. (1998) Neurotransmitter-induced novel modulation of a nonselective cation channel by a cAMP-dependent mechanism in rat pineal cells. *J. Neurophysiol* **79,** 2546–2556 CrossRef Medline
15. Caputo, A., Caci, E., Ferrera, L., Pedemonte, N., Barsanti, C., Sondo, E., Pfeffer, U., Ravazzolo, R., Zegarra-Moran, O., and Galietta, L. J. (2008) TMEM16A, a membrane protein associated with calcium-dependent chloride channel activity. *Science* **322,** 590–594 CrossRef Medline
16. Schroeder, B. C., Cheng, T., Jan, Y. N., and Jan, L. Y. (2008) Expression cloning of TMEM16A as a calcium-activated chloride channel subunit. *Cell* **134,** 1019–1029 CrossRef Medline
17. Yang, Y. D., Cho, H., Koo, J. Y., Tak, M. H., Cho, Y., Shim, W. S., Park, S. P., Lee, J., Lee, B., Kim, B. M., Raouf, R., Shin, Y. K., and Oh, U. (2008) TMEM16A confers receptor-activated calcium-dependent chloride conductance. *Nature* **455,** 1210–1215 CrossRef Medline
18. Kunzelmann, K., Tian, Y., Martins, J. R., Faria, D., Kongsuphol, P., Ousingsawat, J., Thevenod, F., Roussa, E., Rock, J., and Schreiber, R. (2011) Anoctamins. *Pflügers Arch.* **462,** 195–208 Medline
19. Huang, F., Wong, X., and Jan, L. Y. (2012) International Union of Basic and Clinical Pharmacology. LXXXV: calcium-activated chloride channels. *Pharmacol. Rev.* **64,** 1–15 CrossRef Medline
20. Pedemonte, N., and Galietta, L. J. (2014) Structure and function of TMEM16 proteins (anoctamins). *Physiol. Rev.* **94,** 419–459 CrossRef Medline
21. Tien, J., Lee, H. Y., Minor, D. L., Jr, Jan, Y. N., and Jan, L. Y. (2013) Identification of a dimerization domain in the TMEM16A calcium-activated chloride channel (CaCC). *Proc. Natl. Acad. Sci. U.S.A.* **110,** 6352–6357 CrossRef Medline
22. Inayama, M., Suzuki, Y., Yamada, S., Kurita, T., Yamamura, H., Ohya, S., Giles, W. R., and Imaizumi, Y. (2015) Orai1-Orai2 complex is involved in store-operated calcium entry in chondrocyte cell lines. *Cell Calcium* **57,** 337–347 CrossRef Medline
23. Suzuki, Y., Ohya, S., Yamamura, H., Giles, W. R., and Imaizumi, Y. (2016) A new splice variant of large conductance Ca^{2+}-activated K^+ (BK) channel α subunit alters human chondrocyte function. *J. Biol. Chem.* **291,** 24247–24260 CrossRef Medline
24. Suzuki, Y., Tsutsumi, K., Miyamoto, T., Yamamura, H., and Imaizumi, Y. (2017) Heterodimerization of two pore domain K^+ channel TASK1 and TALK2 in living heterologous expression systems. *PLoS ONE* **12,** e0186252 CrossRef Medline
25. Yamamura, H., Ikeda, C., Suzuki, Y., Ohya, S., and Imaizumi, Y. (2012) Molecular assembly and dynamics of fluorescent protein-tagged single $K_{Ca}1.1$ channel in expression system and vascular smooth muscle cells. *Am. J. Physiol. Cell Physiol.* **302,** C1257–C1268 CrossRef Medline
26. Suzuki, Y., Yamamura, H., Ohya, S., and Imaizumi, Y. (2013) Caveolin-1 facilitates the direct coupling between large conductance Ca^{2+}-activated K^+ (BK_{Ca}) and Cav1.2 Ca^{2+} channels and their clustering to regulate membrane excitability in vascular myocytes. *J. Biol. Chem.* **288,** 36750–36761 CrossRef Medline
27. Ohshiro, J., Yamamura, H., Saeki, T., Suzuki, Y., and Imaizumi, Y. (2014) The multiple expression of Ca^{2+}-activated Cl^- channels via homo- and hetero-dimer formation of TMEM16A splicing variants in murine portal vein. *Biochem. Biophys. Res. Commun.* **443,** 518–523 CrossRef Medline
28. Yamamura, H., Suzuki, Y., and Imaizumi, Y. (2015) New light on ion channel imaging by total internal reflection fluorescence (TIRF) microscopy. *J. Pharmacol. Sci.* **128,** 1–7 CrossRef Medline
29. Liu, B., Linley, J. E., Du, X., Zhang, X., Ooi, L., Zhang, H., and Gamper, N. (2010) The acute nociceptive signals induced by bradykinin in rat sensory neurons are mediated by inhibition of M-type K^+ channels and activation of Ca^{2+}-activated Cl^- channels. *J. Clin. Invest.* **120,** 1240–1252 CrossRef Medline
30. Cho, H., Yang, Y. D., Lee, J., Lee, B., Kim, T., Jang, Y., Back, S. K., Na, H. S., Harfe, B. D., Wang, F., Raouf, R., Wood, J. N., and Oh, U. (2012) The calcium-activated chloride channel anoctamin 1 acts as a heat sensor in nociceptive neurons. *Nat. Neurosci.* **15,** 1015–1021 CrossRef Medline
31. Stöhr, H., Heisig, J. B., Benz, P. M., Schöberl, S., Milenkovic, V. M., Strauss, O., Aartsen, W. M., Wijnholds, J., Weber, B. H., and Schulz, H. L. (2009) TMEM16B, a novel protein with calcium-dependent chloride channel activity, associates with a presynaptic protein complex in photoreceptor terminals. *J. Neurosci.* **29,** 6809–6818 CrossRef Medline
32. Stephan, A. B., Shum, E. Y., Hirsh, S., Cygnar, K. D., Reisert, J., and Zhao, H. (2009) ANO2 is the cilial calcium-activated chloride channel that may mediate olfactory amplification. *Proc. Natl. Acad. Sci. U.S.A.* **106,** 11776–11781 CrossRef Medline
33. Billig, G. M., Pál, B., Fidzinski, P., and Jentsch, T. J. (2011) Ca^{2+}-activated Cl^- currents are dispensable for olfaction. *Nat. Neurosci.* **14,** 763–769 CrossRef Medline
34. Huang, W. C., Xiao, S., Huang, F., Harfe, B. D., Jan, Y. N., and Jan, L. Y. (2012) Calcium-activated chloride channels (CaCCs) regulate action potential and synaptic response in hippocampal neurons. *Neuron* **74,** 179–192 CrossRef Medline
35. Pifferi, S., Dibattista, M., and Menini, A. (2009) TMEM16B induces chloride currents activated by calcium in mammalian cells. *Pflügers Arch.* **458,** 1023–1038 Medline
36. Adomaviciene, A., Smith, K. J., Garnett, H., and Tammaro, P. (2013) Putative pore-loops of TMEM16/anoctamin channels affect channel density in cell membranes. *J. Physiol.* **591,** 3487–3505 CrossRef Medline
37. Ferrera, L., Caputo, A., Ubby, I., Bussani, E., Zegarra-Moran, O., Ravazzolo, R., Pagani, F., and Galietta, L. J. (2009) Regulation of TMEM16A chloride channel properties by alternative splicing. *J. Biol. Chem.* **284,** 33360–33368 CrossRef Medline
38. Scudieri, P., Sondo, E., Caci, E., Ravazzolo, R., and Galietta, L. J. (2013) TMEM16A-TMEM16B chimaeras to investigate the structure-function relationship of calcium-activated chloride channels. *Biochem. J.* **452,** 443–455 CrossRef Medline
39. Ohshiro, J., Yamamura, H., Suzuki, Y., and Imaizumi, Y. (2014) Modulation of TMEM16A-channel activity as Ca^{2+} activated Cl^- conductance via the interaction with actin cytoskeleton in murine portal vein. *J. Pharmacol. Sci.* **125,** 107–111 CrossRef Medline
40. Fallah, G., Römer, T., Detro-Dassen, S., Braam, U., Markwardt, F., and Schmalzing, G. (2011) TMEM16A(a)/anoctamin-1 shares a homodimeric architecture with CLC chloride channels. *Mol. Cell. Proteomics* **10,** M110.004697
41. Sheridan, J. T., Worthington, E. N., Yu, K., Gabriel, S. E., Hartzell, H. C., and Tarran, R. (2011) Characterization of the oligomeric structure of the Ca^{2+}-activated Cl^- channel Ano1/TMEM16A. *J. Biol. Chem.* **286,** 1381–1388 CrossRef Medline
42. Dauner, K., Lissmann, J., Jeridi, S., Frings, S., and Möhrlen, F. (2012) Expression patterns of anoctamin 1 and anoctamin 2 chloride channels in the mammalian nose. *Cell Tissue Res.* **347,** 327–341 CrossRef Medline
43. Maurya, D. K., and Menini, A. (2014) Developmental expression of the calcium-activated chloride channels TMEM16A and TMEM16B in the mouse olfactory epithelium. *Dev. Neurobiol.* **74,** 657–675 CrossRef Medline
44. Bernstein, K., Vink, J. Y., Fu, X. W., Wakita, H., Danielsson, J., Wapner, R., and Gallos, G. (2014) Calcium-activated chloride channels anoctamin 1 and 2 promote murine uterine smooth muscle contractility. *Am. J. Obstet. Gynecol.* **211,** 688.e1–10 CrossRef Medline
45. Zhao, L., Li, L. I., Ma, K. T., Wang, Y., Li, J., Shi, W. Y., Zhu, H. E., Zhang, Z. S., and Si, J. Q. (2016) NSAIDs modulate GABA-activated currents via Ca^{2+}-activated Cl^- channels in rat dorsal root ganglion neurons. *Exp. Ther. Med.* **11,** 1755–1761 CrossRef Medline
46. Kitamura, K., and Yamazaki, J. (2001) Chloride channels and their functional roles in smooth muscle tone in the vasculature. *Jpn. J. Pharmacol.* **85,** 351–357 CrossRef Medline
47. Imaizumi, Y., Muraki, K., and Watanabe, M. (1989) Ionic currents in single smooth muscle cells from the ureter of the guinea-pig. *J. Physiol.* **411,** 131–159 CrossRef Medline
48. Ohya, S., Yamamura, H., Muraki, K., Watanabe, M., and Imaizumi, Y. (2001) Comparative study of the molecular and functional expression of L-type Ca^{2+} channels and large-conductance, Ca^{2+}-activated K^+ channels in rabbit aorta and vas deferens smooth muscle. *Pflügers Arch.* **441,** 611–620 Medline
49. Shyu, Y. J., Liu, H., Deng, X., and Hu, C. D. (2006) Identification of new fluorescent protein fragments for bimolecular fluorescence complementation analysis under physiological conditions. *BioTechniques* **40,** 61–66 CrossRef Medline